REDUCING THE EMISSIONS AND EFFICIENCY PENALTIES OF LOW TEMPERATURE COMBUSTION THROUGH LOW HEAT REJECTION OPERATION

A Thesis

by

TIMOTHY HERBERT KROEGER

Submitted to the Office of Graduate and Professional Studies of
Texas A&M University
in partial fulfillment of the requirements for the degree of

MASTER OF SCIENCE

Chair of Committee,	Timothy Jacobs
Committee Members,	Jerald Caton
	Adonios Karpetis
Head of Department,	Andreas Polycarpou

December 2017

Major Subject: Mechanical Engineering

ABSTRACT

Low temperature combustion (LTC) is popular among diesel engine researchers because it dramatically reduces NO_x and smoke emissions. However, LTC is limited by increased CO and hydrocarbon emissions as well as by reduced efficiency. At the same time, low heat rejection (LHR) operation has tantalized researchers with the promise of large efficiency improvements, but it has often failed to meet simulated expectations. Since LHR techniques inevitably increase combustion chamber temperatures, the ratio of specific heats of the cylinder contents is decreased, reducing the potential conversion of thermal energy to work. Combining LTC and LHR allows for low heat transfer losses and a high ratio of specific heats, providing the opportunity for increased efficiency.

An experiment was conducted to evaluate potential improvements to a mild LTC mode's combustion efficiency and thermal efficiency. The experiment used elevated engine coolant temperatures (ECT) to reduce the temperature gradient across the cylinder walls in a 1.9L four-cylinder DI diesel engine. In particular, NO_x, smoke, CO, and hydrocarbon emissions were compared between LTC and conventional conditions over the ECT range (from 90 °C to 120 °C), and various measures of efficiency were compared as well. Elevated coolant temperatures reduced the carbon monoxide and hydrocarbon emissions penalties of the LTC mode, improving LTC combustion efficiency. The thermal efficiency of the mild LTC mode was not significantly different from that of the conventional mode, and brake thermal efficiency for both modes improved at higher coolant temperatures.

DEDICATION

To Brontee, who has been there for me even when she is far away.

ACKNOWLEDGEMENTS

I am especially thankful to Dr. Jacobs for guidance and support through several years and several projects, starting in my sophomore thermodynamics course. His guidance helped me through two projects during my master's degree, as well as through the ordeal of getting the test cell up and running again. I am also grateful to my committee members, Dr. Caton and Dr. Karpetis, for their willingness to help and kindness during this process.

I am grateful for my fellow students in the Advanced Engine Research Lab, especially Jeff Brown, Cole Frazier, Jue Li, and Ben McKeathen for their extensive help at various stages of the project. I must also thank the professors and staff in the mechanical engineering department for their accessibility, helpfulness, and support throughout my education. And I am most thankful for my family and for Brontee, who always want what's best for me and who support me in everything I do.

CONTRIBUTORS AND FUNDING SOURCES

This work was supervised by a thesis committee consisting of Professor Timothy Jacobs and Professor Jerald Caton of the Department of Mechanical Engineering and Professor Adonios Karpetis of the Department of Aerospace Engineering. All work for the thesis was completed by the student, under the advisement of Professor Timothy Jacobs of the Department of Mechanical Engineering.

Graduate study was supported by the Graduate Merit Fellowship from Texas A&M University and the National Science Foundation Graduate Research Fellowship Program under Grant No. DGE-1252521. This work was made possible in part by the National Science Foundation under Grant Number 1343255. Any opinion, findings, and conclusions or recommendations expressed in this material are those of the author and do not necessarily reflect the views of the National Science Foundation.

NOMENCLATURE

ATDC	After Top Dead Center
BTDC	Before Top Dead Center
CA	Crank Angle
CA50	Crank Angle Location of 50% Mass Fraction Burned, ATDC
CI	Compression Ignition
CO	Carbon Monoxide
DAQ	Data Acquisition (can also stand for Data Acquisition System)
DEF	Diesel Exhaust Fluid
ECT	Engine Coolant Temperature
ECU	Engine Control Unit
EGR	Exhaust Gas Recirculation
FSN	Filter Smoke Number
FID	Flame Ionization Detector
HC	Hydrocarbon
HCCI	Homogeneous Charge Compression Ignition
IR	Infrared
LHR	Low Heat Rejection
LTC	Low Temperature Combustion
MFB	Mass Fraction Burned
NB	Nota Bene

NDIR	Non-Dispersive Infrared
NO_x	Oxides of Nitrogen
OEM	Original Equipment Manufacturer
PCCI	Premixed Charge Compression Ignition
RCCI	Reactivity Controlled Compression Ignition
ROHR	Rate of Heat Release
SI	Spark Ignited
TDC	Top Dead Center
THC	Total Hydrocarbons

TABLE OF CONTENTS

Page

LIST OF FIGURES

Page

LIST OF TABLES

1. INTRODUCTION

1.1. Motivation

Diesel engines are popular in myriad applications largely because they are more efficient than their spark ignition counterparts [1]. However, diesel engines produce significant amounts of several important pollutants [1, 2]. One primary goal shared by engine researchers is to increase efficiency and decrease emissions. With NO_x emissions and smoke (or particulate matter in general) typically occurring in the most concerning concentrations, LTC has been developed which simultaneously reduces NO_x and smoke [2, 3]. A downside of LTC has often been that it produces higher levels of total hydrocarbon and CO emissions and that it degrades efficiency [2-5]. The motivation of this study is to reduce the drawbacks of the LTC mode, returning high efficiency and low emissions through the addition of the LHR technique.

1.2. Background

In order to understand the present study, it is important to know the processes responsible for NO_x and soot emissions. Once the soot-NO_x tradeoff is explained, the LTC modes discussed in the literature review will make more sense.

1.2.1. NO_x Formation

Conventional IC engine fuels, including diesel, do not contain appreciable nitrogen. Instead, the diatomic nitrogen in air provides the nitrogen molecules which react to form NO_x. Four mechanisms describe NO_x chemistry, namely the Zeldovich, Fenimore, N_2O-intermediate, and NNH mechanisms [6]. Under the conditions found in a

diesel engine, NO_x formation is well characterized by the extended Zeldovich mechanism, comprised of three reactions [1, 6, 7].

$$O + N_2 \leftrightarrow NO + N \quad (1)$$

$$N + O_2 \leftrightarrow NO + O \quad (2)$$

$$N + OH \leftrightarrow NO + H \quad (3)$$

This mechanism is highly dependent on temperature, with negligible NO_x formation below about 1800 K [6]. This is a key advantage of low temperature combustion techniques: they target peak in-cylinder temperatures below the threshold for substantial NO_x. Under low-temperature regimes, the N_2O-intermediate mechanism may become more important than the Zeldovich mechanism, but experiments show low NO_x for diesel LTC engine operation [2, 3, 6, 8].

1.2.2. Soot Formation

Soot is carbonaceous particulate matter that results from incomplete combustion. Soot dominates the composition of particulate matter (which can have other sources as well) under these conditions [1, 6]. Condensed, unburned hydrocarbons are the second-most important component of diesel particulate matter [6]. The formation and destruction of soot in diesel engines is dependent on in-cylinder temperature and equivalence ratio.

In typical DI diesel operation, soot forms in high concentrations in the locally fuel-rich core of a diesel fuel spray [1]. Then, most of this soot is oxidized as it comes in contact with oxidizers in the more globally fuel-lean chamber prior to exhaust [1]. Because of this obvious effect of mixing, soot formation is a hallmark of non-premixed

(diffusion) flames [6]. A pre-mixed lean flame will form less carbonaceous soot. Therefore, paraphrasing Turns, in-cylinder strategies to control soot must rely on reducing formation and/or increasing oxidation [6].

This leads to discussion of temperature's effect on formation and oxidation processes. For a given equivalence ratio, the formation and oxidation rates are represented by Figure 1 reproduced from Jacobs [9]. For high temperatures, the rate of oxidation approaches the rate of formation, so the net release of soot begins to decrease.

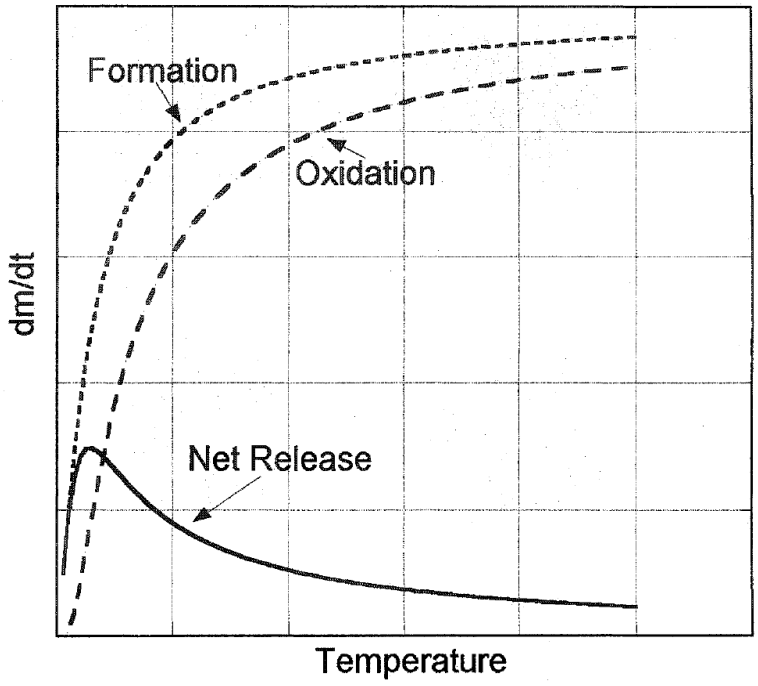

Figure 1: Formation, oxidation, and net release rates of soot with respect to temperature [9].

Conventional diesel combustion occurs in the moderate and high temperature portions of Figure 1, where an increase in temperature causes a decrease in soot.

However, it is also established that the same increase in temperature would *increase* NO_x emissions. This is the infamous soot-NO_x tradeoff of conventional diesel combustion. Operating conditions which decrease soot tend to increase NO_x and vice versa. Fortunately, the left-most portion of Figure 1 reveals a path to defeat the soot-NO_x tradeoff. If temperatures are much lower than the conventional regime, then the net release of soot may also be reduced. Thus, sufficiently low temperatures in the combustion chamber can provide low emissions of both soot and NO_x.

1.3. Objective

This study is a successor to two previous studies, one by Caton and the other by Penny [8, 10]. These and other literature on LTC and/or LHR will be discussed next, but the basic premise of this experiment is simple. The LHR condition traps more thermal energy in the combustion chamber during combustion and expansion. Through the LTC mode, lower combustion temperatures can provide a higher ratio of specific heats for the cylinder contents, increasing the efficiency of the expansion stroke [10]. Penny established a suitable LTC mode by experiment, a variation of which was used in the present study [8]. However, to reduce the risk of high-temperature-related damage to engine components, Penny actually observed a *high* heat rejection mode, wherein test cases ranged from higher-than-normal down to normal levels of engine heat rejection [8]. Penny's methodology established important proof-of-concept trends—which will be reviewed with the rest of the literature—but it did not truly explore an LHR regime to couple with the LTC mode.

The objective, then, is to validate Caton's simulation study by combining an LTC mode and Penny's methodology with a true LHR regime. The LTC-LHR mode will be evaluated for changes in various emissions and efficiency metrics. These include NO_x, soot, CO, and THC emissions, and combustion, net indicated, brake thermal, and brake fuel conversion efficiencies. Based on the implications of Caton's study, it is desired that combustion efficiency and thermal efficiency can be improved for an LTC mode through this LHR technique.

2. LITERATURE REVIEW

2.1. Overview

Apart from Penny and Caton, few researchers have sought to combine LTC and LHR techniques. Therefore, this literature review will begin with an overview of LTC and the various techniques by which it is achieved. Then, the review will focus on LHR engines, including discrepancies among various experimental results and especially between experimental and computational results. Prior LTC-LHR combined research will also be discussed.

2.2. Low Temperature Combustion

While all LTC techniques seek to defeat the soot-NO_x tradeoff, there are important differences in how each technique achieves this condition. The three primary techniques are HCCI, PCCI, and RCCI. Besides defeating the soot-NO_x tradeoff, these techniques offer different advantages and drawbacks.

High EGR fractions are important to achieving the LTC outcome through any of these techniques. EGR is useful because it acts as a heat sink during combustion, further reducing peak temperature. In conventional diesel engines, some EGR is applied to reduce NO_x [1, 11]. But in the context of LTC, this effect is coupled with EGR's tendency to prolong ignition delay, which aids pre-mixing and thereby can also reduce soot formation [4, 12, 13]. Thus, combined with high levels of EGR, the following techniques can achieve LTC conditions to circumvent the soot-NO_x tradeoff. Downsides

of EGR include increased HC emissions [1, 14], as well as potential for poorer engine breathing for high levels of EGR [12].

2.2.1. HCCI

In the HCCI technique, fuel is introduced early enough (for example, by port injection during intake) to create a homogeneous mixture of fuel and air, similar to the charge in a conventional SI engine [14]. However, unlike the conventional, near-stoichiometric SI case, the HCCI mixture is quite lean. When this well-mixed lean mixture is compressed, it eventually reaches its autoignition point. Because the reactants are well-mixed and other gradients in the cylinder are rather small during the compression stroke, combustion occurs rapidly and simultaneously throughout the chamber [13, 14]. Because the fuel is well-mixed with air, the local equivalence ratio during HCCI combustion is the same as the global equivalence ratio, which is markedly untrue in conventional diesel combustion [14]. Locally lean combustion seen in HCCI occurs at a substantially lower temperature than locally stoichiometric or locally rich combustion which may occur in conventional diesel operation, and this lower temperature leads to low NO_x. The lean, well-mixed charge also contributes to low soot emissions, since soot formation is known to be exacerbated by mixing-controlled combustion and fuel-rich regions [1, 6, 14].

The rapid rate of HCCI combustion can also lead to improved thermal efficiency when properly phased, since the nearly instantaneous combustion process can approximate the Otto cycle's heat release [13, 14]. Unfortunately, HCCI can also suffer from increased CO and HC emissions, which is attributed to LTC itself as well as to

liquid fuel impingement on the walls [14-16]. With lower temperature combustion, the flame can more easily be quenched near the edges of the chamber, leading to products of incomplete combustion [14, 16, 17]. Additionally, since temperatures remain lower throughout the combustion and expansion stroke, these incomplete products never have an opportunity to be completely oxidized later in the stroke [14]. (In a conventional engine operating mode, unburned gases from a quenched region would have some opportunity to diffuse into hotter regions of the chamber and be fully oxidized [16].) The other main contributor to incomplete combustion is liquid fuel impingement on the combustion chamber, which of course exacerbates the problems associated with flame quenching [14, 15]. The negative impact of HCCI on combustion efficiency can potentially overcome any gains in thermal efficiency, leading to a decrease in fuel conversion efficiency (or an increase in specific fuel consumption) [11, 14].

The main challenges of implementing the HCCI technique are control of combustion phasing and restrictions on engine load [8, 13, 14]. Controlling the ignition timing is difficult without the spark ignition or injection timing control present in conventional gasoline and diesel engines, respectively [14]. Of course, spark ignition is not an option, since the key distinction between HCCI and conventional SI operation is simultaneous compression ignition throughout the mixture, rather than flame front propagation from a spark. And HCCI injection timing does not directly correspond to ignition delay—as it may in a conventional diesel engine—because fuel must be introduced early enough to achieve homogeneity before the mixture nears its autoignition point. Stanglmaier and Roberts give many examples of factors which

influence HCCI combustion phasing, including fuel properties, equivalence ratio, residual/EGR fraction, intake temperature, heat transfer to/from the engine, and others [14]. Additionally, HCCI suffers from both a floor and a ceiling governing its useful load. The minimum load is restricted by the lean flammability limit of the fuel because it is well mixed. At higher loads, the pressure rise rate increases, which can damage the engine, and the emissions benefits diminish [13, 14].

2.2.2. PCCI

PCCI is largely similar to HCCI, with a goal of creating a substantially mixed, lean charge such that locally lean, non-diffusion-limited LTC occurs. PCCI generally refers to an operating mode that achieves partial pre-mixing or a stratified charge, rather than a homogeneous mixed charge throughout the chamber [8]. A successful PCCI mode could be a DI engine with a prolonged ignition delay to provide sufficient mixing throughout the fuel spray for combustion, although the vaporized fuel would not necessarily be diffused throughout the chamber into a homogeneous fuel-air mixture everywhere. In a DI PCCI engine, there are two possible injection strategies: substantially advanced or substantially retarded fuel injection. Either injection strategy serves to lengthen the ignition delay, giving the fuel spray more time to entrain air and become mixed prior to autoignition. The increase in ignition delay with advanced timing is rather obvious: earlier in the compression stroke, the fuel has longer to mix before any portion of the charge is compressed to the point of autoignition. However, the retarded timings can be even more useful for attaining LTC because “the increase in ignition delay as timing is retarded from the location of minimum ignition delay is greater than

that as timing is advanced from the same location" [2]. Retarded injection avoids fuel impingement on cylinder walls, which is a problem associated with very advanced injection [2, 3].

Although the mixture is not homogeneous as in HCCI operation, the PCCI technique provides a sufficiently well-mixed fuel spray to result in rapid pre-mixed combustion without the mixing-controlled diffusion flame seen in conventional diesel operation. Therefore, the benefits and downsides of PCCI combustion are also similar to HCCI. Namely, PCCI must contend with elevated HC and CO emissions [4, 8, 18]. PCCI is also limited to low load conditions, albeit for a different primary reason than HCCI. With PCCI, longer injection durations at high load inevitably lead to substantial diffusion-limited combustion, eliminating the desired premixed combustion effect [11, 18].

2.2.3. RCCI

RCCI adds complexity to the LTC formula by using two fuels, inducting/injecting them separately and allowing the fuels to interact in-cylinder. Penny provides a good, simple explanation of the idea, paraphrased here. First, a less reactive fuel such as gasoline (which resists autoignition) is inducted via port injection. Then, a more reactive fuel like diesel is directly injected [8]. The relative quantities of the two fuels—as well as the timing of the diesel injection—provides more control over combustion phasing [8, 12, 19]. Improved control of the ignition timing enables a wider range of applicable loads, which is a major advantage over PCCI and HCCI [12]. Emissions are similar to HCCI and PCCI: low soot and NO_x, but high CO and HC [12,

19]. The complexity of a dual-fuel system can be mitigated to a system requiring a single fuel and a relatively small amount of reactivity-influencing additive, which would make the technique more palatable to consumers (who already deal with technologies like DEF). For example, small amounts of cetane-increasing additives can be used with a gasoline-only system to increase reactivity during the direct injection phase [20, 21].

2.3. Low Heat Rejection

To remedy the important drawbacks of LTC operation, Caton proposed that combining LHR techniques with LTC could realize improved efficiency [10]. Low heat rejection engines have been studied for decades, since researchers expected substantial improvements in efficiency by removing cylinder heat rejection as a source of energy losses [22-24]. However, while insulating the cylinder head, cylinder liner, and/or piston crown sometimes caused reductions in fuel consumption, insulation often failed to yield the improvements predicted by simulations [22]. Still other experimental studies found that fuel consumption actually increased when cylinders were insulated [25, 26].

Woschni and Spindler posited the application of *combustion vive* to insulated diesel engines as an explanation of such degraded performance [27]. This phenomenon refers to a sharp increase in the combustion gas to cylinder wall heat transfer coefficient due to the thinning of the thermal boundary layer with elevated wall temperatures [27, 28]. This claim of increased heat rejection with insulated diesel engine combustion chambers was specifically disputed by Cheng and Wong [29]. Other experimental results conflict with the *combustion vive* hypothesis simply by displaying reduced heat rejection [30-32].

A more easily verified reason for poor LHR experimental performance is degraded volumetric efficiency [22-24]. In successful experiments (those for which fuel consumption decreased compared to the baseline engine), A/F ratio was maintained by turbocharging or charge cooling [30, 31]. For unsuccessful cases, the insulated chamber resulted in higher air temperatures during the intake period, causing reduced A/F ratio and poorer performance [25, 26].

Even with special care taken to achieve constant A/F ratio, experimental results often failed to achieve the large benefits suggested by simulations [22]. In fact, most energy recouped by LHR techniques manifested itself as available exhaust energy, which meant that turbocompounding was key to the most successful LHR engines [22, 33]. Turbocompounding allows LHR engines to extract shaft work from the exhaust rather than directly through improved cycle efficiency.

Caton proposed that previous LHR studies were limited in their cycle efficiency by the combustion gases' ratio of specific heats [10]. Because insulation causes higher combustion chamber temperatures, the ratio of specific heats normally decreases with LHR techniques, which leads to poor conversion of thermal energy to work [10]. In the LTC regime, the benefits of low heat rejection might be realized by maintaining low enough temperatures to allow a non-limiting ratio of specific heats [10].

Simulations by Caton found that LHR techniques improved the brake thermal efficiency of the LTC regime, and experimental work by Penny found that LHR-LTC operation causes brake thermal efficiency, as well as CO and THC emissions, to approach conventional combustion levels even though NO_x and smoke emissions remain

low [8, 10]. Penny reduced heat rejection by elevating engine coolant temperature instead of by insulating the combustion chamber [8]. However, Penny's work actually explored mostly below-average coolant temperatures in order to establish trends with increasing temperature [8]. The maximum temperature of his study was only 100°C, a slight elevation from normal conditions [8].

This study expands upon Penny's prior work by exploring elevated coolant temperatures up to 120°C, thereby more significantly reducing heat rejection from the combustion chamber. The study aims to maintain significantly reduced NO_x emissions and conventional smoke levels while improving the CO emissions, hydrocarbon emissions, and brake thermal efficiency of the LTC regime through elevated engine coolant temperatures.

3. EXPERIMENTAL APPARATUS AND METHODS

3.1. Engine and Controller

The test engine is a General Motors 1.9L four-cylinder direct injection diesel engine with a variable geometry turbocharger, common rail fuel injection system, and exhaust gas recirculation. The engine's specifications are provided in Table 1. The cooled EGR loop, high pressure common rail, and electronically controlled direct injection are important technologies for this study. Another important element of this research is the electronically controlled (not mechanically driven) radiator fan, which allows for control of ECT.

Table 1: Description of test engine characteristics.

Parameter	**Value**
Bore	82 mm
Stroke	90.4 mm
Displacement	1.91 L
Rated Power	110 kW at 4000 rpm
Rated Torque	315 N-m at 2000-2750 rpm
Compression Ratio	18:1 (nominal)
Fuel System	High Pressure Common Rail
Pump	Mechanically Driven
Injection	Electronic, Direct Injection
Aspiration	Turbocharged with EGR
Turbocharger	Variable Geometry

A third-party controller regulates common rail fuel pressure, fuel injection timings and durations, EGR, and radiator fan speed. Additionally, a DC dynamometer

controls engine speed and can motor the engine. The dynamometer is also equipped with a load cell to measure brake torque.

The engine test cell is shown schematically in Figure 2. Important features are the EGR loop, turbocharger, dynamometer, and emissions measurement equipment.

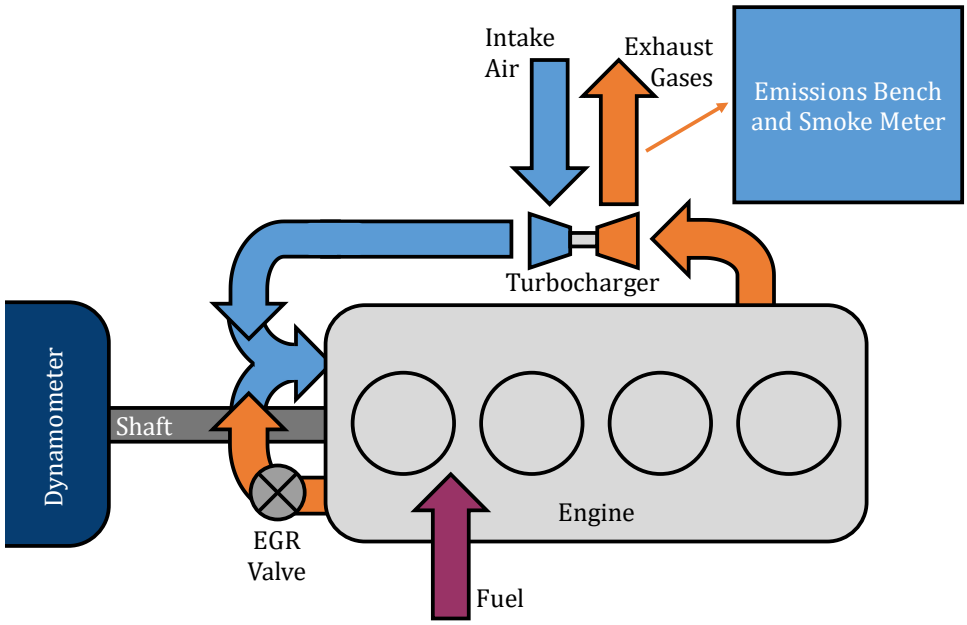

Figure 2: Schematic of test cell featuring equipment and mass flows.

The EGR valve can be electronically controlled to allow or restrict recirculation of exhaust gases. Fuel is provided through a filter and two external low-pressure pumps in series, which feed the engine's stock high-pressure pump. The fuel flows from the high-pressure pump to the common rail, then to individual injectors. Small samples of exhaust gases flow to the emissions bench and the smoke meter, with the rest exiting the

laboratory through a main exhaust pipe. The intake air comes from an elevated filter box to reduce the load of dust and other particles on the air filter.

3.2. Fuel

Number 2 petroleum diesel was used for all testing. While this drum of fuel has not been analyzed, it is similar to the batch previously analyzed for use in engine research at Texas A&M University. The properties obtained from a third party analysis for that previous study are presented in Table 2, and some of these values are used in subsequent calculations requiring fuel properties.

Table 2: Properties of No. 2 diesel fuel.

Property	**Units**	**Value[a]**
Density	kg/m^3	825.5
Net Heating Value	MJ/kg	43.008
Gross Heating Value	MJ/kg	45.853
Sulfur	ppm	5.3
Viscosity	cSt	2.247
Cetane Number	-	51.3
Hydrogen	wt. %	13.41
Carbon	wt. %	85.81
Oxygen	wt. %	0.78
Initial Boiling Point	°C	173.4
Final Boiling Point	°C	340.5

[a] Measured or calculated by Southwest Research Institute (San Antonio, TX)

Uncertainty from applying these properties (from a different batch of similar petroleum diesel) is expected to be small compared to uncertainty from instrumentation and day-to-day test variations. For instance, 43 MJ/kg ± 1% is widely used as the net heating value of diesel fuel, regardless of batch [1, 34].

3.3. Measurements and Data Acquisition

3.3.1. OEM Engine Sensors

The original suite of sensors supplied for the engine's use in an automotive role are still useful in the research lab. The third-party controller and DAQ systems used in the lab feature an interface with these sensors, which would otherwise communicate with an ECU in an automobile. For instance, intake air flow rate, EGR valve position, common rail fuel pressure, and engine coolant temperature are provided by these stock sensors and are particularly important for control of the engine in this experiment.

3.3.2. In-Cylinder Pressure Transducers

Crank angle resolved in-cylinder pressure is important for many aspects of engine research (such as determining burn rates). The engine is equipped with ports for glow plugs, which are not needed in the laboratory setting. Instead, Kistler piezoelectric pressure transducers are installed in those ports. In-cylinder pressure is correlated to crank angle via an optical encoder with a resolution of 0.2 °CA. These transducers are periodically removed and calibrated with a separate hydraulic tool, and during engine operation it is easy to verify if the motoring curves for each cylinder line up. During data acquisition, 200 consecutive cycles are recorded and the results are ensemble averaged to provide a representative pressure trace. Averaging 200 consecutive cycles can

mitigate the impact of random cyclic variation, since—for instance—aberrant cycles of high peak pressure will likely be canceled out on average by cycles of low peak pressure.

3.3.3. Exhaust Analyzers

Important components of the engine emissions are measured by a Horiba MEXA-7000 emissions bench and an AVL smoke meter. NO_x is measured by the chemiluminescence technique. Measuring combined NO_x was desirable in this study, since ultimately all NO will proceed to NO_2 in the environment [6]. Combined NO_x concentration is therefore relevant since it effectively describes how much NO_2 would end up in the atmosphere under these conditions. Since the chemiluminescence technique only quantifies NO concentration, all the NO_2 in the raw sample must be converted to NO before entering the analyzer [35, 36]. An ozone generator in the emissions bench creates O_3, which reacts with NO to form O_2 and an excited state of NO_2 [35]. The excited NO_2 releases light as it returns to a ground state, and the quantity of photons released by the NO_2 is proportional to the amount of NO entering the analyzer [35]. Spanning against a calibration gas of known NO concentration sets the proportionality constant, with manufacturer-provided calibration curves to address non-linearity in the useful range.

CO and CO_2 are both measured by a non-dispersive infrared technique. This method makes use of the absorption of IR light at unique wavelengths for particular gas molecules [37]. There are a few variations on available NDIR analyzers, such as how cross-sensitivity to other gases is mitigated and how the sensor is calibrated to the

concentration of the target gas [38]. The Horiba MEXA bench has two NDIR analyzers: one for low concentrations of CO, and the other for CO_2 and high concentrations of CO [36]. Measurement of two gases by one analyzer is achieved through a chopper wheel with a reference filter and a filter for each target gas, so that a single IR detector can alternately measure each concentration as the wheel rotates [36]. A separate reference cell of non-absorbing gas (N_2) parallel to the sample cell is used to provide the baseline IR intensity with no absorption [36]. Then, the Beer-Lambert Law is used to calculate the target gas concentration based on known baseline intensity, absorption coefficients of the target gases, and absorption path length [37, 38]. The sample is dried to prevent cross-sensitivity of CO with water vapor. The analyzer also includes a second detector designed to compensate for interference [36].

Hydrocarbon emissions are measured by a flame ionization detector. The FID analyzer quantifies the release of ions by the combustion of hydrocarbons in a hydrogen-air flame. A pair of electrodes with a DC bias voltage are used, with one electrode acting as the ion collector; the other electrode is the nozzle from which the sample flows [39-42]. The current across the electrodes is proportional to the rate of ionization [36, 40, 42, 43]. Since production of ions is proportional to the carbon concentration in the exhaust hydrocarbons, the current in the FID is proportional to the concentration of hydrocarbons. This method works excellently for molecules containing only carbon and hydrogen (such as CH_4), but it works poorly for other organic molecules such as formaldehyde (CH_2O) [42]. The FID method does not respond to CO and CO_2 for the same reason, as they are partially and fully oxidized, respectively [39, 42]. An important

benefit of FID measurements is that they have a linear response over a wide range of hydrocarbon concentrations [36, 42, 43].

Soot concentration in the exhaust is represented by the FSN measured in the smoke meter. The smoke meter passes a defined sample volume heated exhaust through a portion of filter paper. Then, an optical technique involving a light source and a reflectometer calculates the paper blackening. Since sample volume is always known but can vary with test conditions, an effective length is defined to correct the measured paper blackening for different sample volumes. The volume-corrected paper blackening measurement is known as FSN [44, 45].

3.3.4. Calibration and General Notes on Uncertainty

Calibration of the in-cylinder pressure transducers was mentioned in ***3.3.2.*** Additionally, the MEXA bench analyzers require frequent, routine adjustments. To begin each day of testing, the MEXA bench analyzers are zeroed and spanned against a reference gases of known concentration. Calibration curves for linearization of nonlinear detection methods are factory installed, but the frequent zeroing and spanning of sensors reduces uncertainty.

Uncertainty is also impacted by ambient conditions, including temperature, pressure, and humidity, since the engine breathes ambient air. To demonstrate repeatability from the experiment despite changes in atmospheric conditions, the full experimental matrix is conducted twice, on different days.

In this document, uncertainty bars on figures represent a 95% confidence interval calculated from the z distribution (which assumes that sample standard deviations reflect population standard deviations).

3.4. Experimental Plan

The experimental plan was designed to encompass two distinct perspectives on data collection and analysis. The first method employed fixed injection timings for the two modes (conventional and LTC) across all coolant temperatures. This kept injection conditions more similar at the expense of matching combustion phasing.

However, as the coolant temperature increases, combustion phenomena are expected to change as well. This means that fuel injected into the cylinder at the same time for two different engine coolant temperatures could burn at two different rates. The change in burning rate could change cycle efficiency and emissions. Therefore, the second part of the experiment was intended to match combustion phasing rather than injection timing. After the first experiment with constant injection timings, it turned out that the second experiment was not necessary. There was no substantial change in combustion phasing (CA50) with respect to coolant temperature, which is discussed further in **4.1.**

3.4.1. Constant Injection Timings

Test conditions (such as load, rail pressure, and speed) follow a methodology similar to Penny, but using higher-than-normal coolant temperatures [8]. The baseline case of conventional combustion was chosen to be a low load condition (~2 bar BMEP) with a rail pressure of 425 bar, a speed of 1500 rpm, and an engine coolant temperature

of 90°C at an injection timing of 8°bTDC. LTC, having already been characterized through injection timing and EGR sweeps for this engine by Penny, was established for an injection timing of 1.5°bTDC and a high EGR level, targeting about 35% [8]. As discussed below (***3.4.2***), a confluence of problems reduced the EGR level in this experiment, rendering a more mild LTC treatment than the version targeted by Penny. Fuel injection duration, fuel rail pressure, and engine speed were held constant throughout the test matrix. LTC and conventional modes were tested with ECT at 90°C, 100°C, 110°C, 115°C, and 120°C. This test plan is documented in Table 3.

Table 3: Test matrix, showing shared speed, rail pressure, and injection duration, with different EGR and injection timings for a range of engine coolant temperatures. The rail pressure and injection duration correspond to a load of nominally 2 bar BMEP.

Speed [rpm]	**Rail Pressure [bar]**	**Injection Duration [ms]**	**EGR Level**	**Start of Injection [°bTDC]**	**Engine Coolant Temperature [°C]**
1500	425	0.75	None	8	90
					100
					110
					115
					120
			22%	1.5	90
					100
					110
					115
					120

As mentioned in **3.3**, measurements at each test condition occurred for 200 consecutive cycles to reduce the impact of cycle-to-cycle variation, and this experiment was repeated over two days to account for the effects of changing ambient conditions from day to day.

3.4.2. Notes on EGR Level

Hardware, software, and user errors combined to prevent EGR level from reaching the initial target of 35%, despite some indications in the DAQ system that the EGR was flowing as desired. After discovering the existence of these problems, the test conditions were repeated, unchanged, at 90 °C and 120 °C to accurately calculate the EGR fraction obtained in the experiment. To correctly measure EGR, an additional sample line just downstream of the junction of intake air and EGR pipes was routed to the emissions bench. The intake concentration of CO_2 is compared against the exhaust concentration of CO_2 to establish a dilution ratio of the intake charge [1, 8]. Then, the mass fraction of EGR in the intake gases is calculated from this dilution ratio and the measured exhaust sample composition [1, 8].

The actual EGR fraction for the LTC cases during the experiment was 22%. One might expect that this relatively moderate EGR level would prevent an LTC condition from existing. However, diagnostic evidence of the LTC condition was present: namely, the defeat of the soot-NO_x tradeoff. As will be shown in ***4.3.1***, substantial reduction in NO_x was achieved without commensurate increase in smoke number. This indicates that the EGR level was sufficient to achieve a mild LTC mode. A more aggressive LTC condition—with even lower NO_x but no higher soot emissions—could be achieved for a

higher EGR fraction, but for this investigation, the defeat of the soot-NO_x tradeoff is a sufficient demonstration of LTC behavior.

3.5. Calculations

3.5.1. Brake Specific NO_x

Since NO_x emissions represent both an indicator and a benefit of LTC operation, it is important to represent NO_x in a way that allows different operating conditions to be compared fairly. As efficiency changes with operating conditions, perceived improvements in NO_x emissions on a volume fraction basis could be misleading—engine processes with different efficiencies would ultimately produce different masses of harmful exhaust gases to provide the same useful work. It is better to represent NO_x output in terms of the useful output of the device, such as grams per kilometer traveled or, more generally, grams per kilowatt-hour. Brake specific NO_x accounts for the mass of NO_x per unit of brake work, as shown in Equation 4.

$$BSNO_x = \frac{(\dot{m}_{air} + \dot{m}_{fuel})Y_{NO_x}}{\dot{W}_{brake}}\left(\frac{MW_{NO_x}}{MW_{exh}}\right) \quad (4)$$

Because NO from NO_x is rather quickly converted to NO_2 in the atmosphere, it is conventional to use the molar mass of NO_2 to represent the molar mass of NO_x [6, 46].

3.5.2. Apparent Rate of Heat Release

The emissions and efficiency of an IC engine are affected by the rate of heat release during the combustion process. Diesel combustion is often characterized as a combination of two phenomena: fast premixed combustion followed by slower mixing-controlled combustion [47]. For just one example of the importance of these phenomena,

soot formation is influenced strongly by the proportions of premixed and mixing-controlled combustion [1, 6]. Therefore, ROHR is an important analysis tool for diesel engine research. The apparent ROHR can be estimated from measured in-cylinder pressure and engine geometry [1]. Using the closed cylinder contents as a control mass, the First Law of Thermodynamics provides the apparent ROHR. The conversion of chemical energy to thermal energy by combustion can be modeled as heat transfer into the control volume, as shown in Figure 3, where δQ_{HR} is the apparent ROHR stand-in for combustion, δQ_{HT} is the heat transfer through the cylinder walls, δW is the boundary work from piston motion, and dU_{CV} is the internal energy of the cylinder contents.

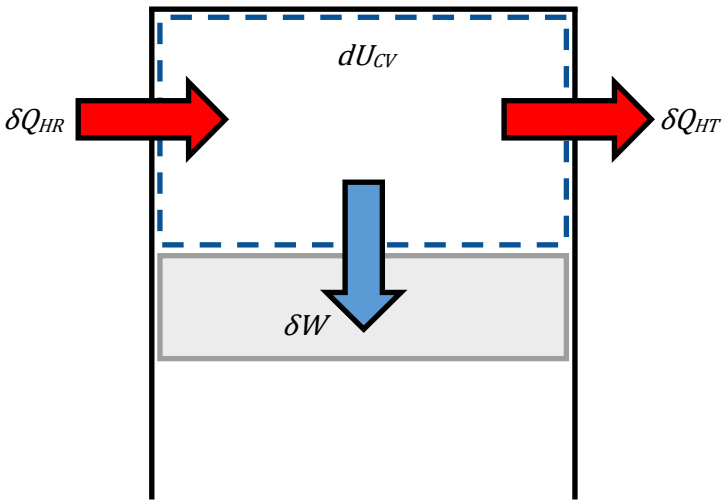

Figure 3: Schematic of cylinder showing energy content and transfers

Applying the First Law of Thermodynamics to the combustion chamber from Figure 3, the apparent ROHR is given by Equation 5.

$$\delta Q_{HR} = \delta W + dU_{CV} + \delta Q_{HT} \quad (5)$$

The heat transfer through the cylinder walls can be modeled through empirical correlations, with the Hohenberg correlation used for the heat transfer coefficient in these results [48]. Boundary work can be calculated from the measured in-cylinder pressure and known piston-cylinder kinematics. By assuming the cylinder gases behave ideally, the internal energy of the cylinder contents can be represented through the known pressure and volume as well, rather than the unknown (and actually non-uniform) in-cylinder temperature [1]. The method and use of this calculation are well-established in the field, with clear explanation from Heywood [1]. Apparent ROHR analysis is a qualitative tool, given the assumptions and heat transfer model required to obtain ROHR. This means that ROHR shows important phenomenological differences related the combustion process without necessarily revealing the absolute magnitudes of energy conversion.

3.5.3. Propagation of Uncertainty

Mean values and standard errors were calculated in the usual way for the outputs from the data acquisition system—such as fuel flow rate or exhaust CO concentration. However, other important parameters—such as the various efficiency metrics—are derived from measured values. In these cases, in which DAQ outputs become the inputs to subsequent calculations, it is important to account for the way uncertainty propagates through that calculation. The standard Kline-McClintock approach for uncertainty propagation uses the root sum square of the various uncertainty contributions [49, 50].

Using a simple example of a function of two variables, z=f(x, y), the estimated variance (s^2) of z is given by Equation 6.

$$s_z^2 = \left[\frac{\partial z}{\partial x}\right]^2 s_x^2 + \left[\frac{\partial z}{\partial y}\right]^2 s_y^2 \quad (6)$$

The derivatives are evaluated at the sample average values of the input parameters. Terms containing a squared derivative and a variance continue to be added for each additional input parameter. The estimated standard deviation of the desired output parameter, then, is the square root of the sum of those squared terms. Using the calculated standard deviations from the Kline-McClintock technique, confidence intervals can be obtained.

3.5.4. Rough Estimate of Combustion Chamber Wall Temperature

As part of the discussion on the hypothesis that LTC thermal efficiency can be improved through LHR due to the relatively high ratio of specific heats during expansion under LTC conditions, a simplified approximation of coolant temperature effect on combustion chamber wall temperature was performed. This analysis was of secondary importance, with the objective of demonstrating that ECT-based LHR technique does not cause the drastic wall temperature increase analyzed by Caton's simulations [10]. To that end, simplifying assumptions were applied.

First, the heat transfer rate to the coolant throughout the entire engine was used. This rate was calculated from measured coolant flow rate and measured radiator temperature difference. It includes heat addition to the coolant due to friction, neglects heat loss from the coolant outside the radiator, and is a steady state measurement, not

reflecting the time-dependent heat transfer during the combustion and expansion processes. Furthermore, it accounts for all cylinders, and dividing total coolant heat transfer evenly among the four cylinders does not account for the fact that different cylinders have slightly different heat transfer and material temperature profiles. However, the inaccuracy introduced by using this overall heat transfer to the coolant is assumed to be small relative to the alternative, which would require estimating in-cylinder averaged gas properties to calculate a time-averaged gas side heat transfer coefficient from correlations intended for the instantaneous heat transfer coefficient.

Another major simplification was the application of 1-dimensional conduction analysis to the cylinder. The cylinder head and liner (both of which transfer heat to the water jacket) were analyzed as plane walls (with the liner being flattened from a cylinder's lateral surface area to a plane of the same thickness) in parallel. Heat transfer to the piston was neglected since the pathway from the piston to the coolant is complicated and the rough magnitude of temperature change can be rather conservatively captured by reducing the evaluated heat transfer surface area, which results in higher analyzed heat flux to combustion chamber surfaces. A higher heat flux is a conservative estimate in this case because higher calculated wall temperatures would tend to disprove the conjecture that experimental conditions experience a smaller increase in wall temperature than Caton's example.

The thicknesses of the cylinder liner and cylinder head from the combustion chamber to the water jacket were previously measured for a separate engine modeling

effort. The cylinder stroke and bore are also known, with half the stroke being used to compute an average exposed cylinder liner area.

Properties of the 50/50 water and ethylene-glycol mixture were obtained from an online lookup table for a temperature of 105 °C, which is in the middle of the range of tested coolant temperatures [51]. Property changes within ±15 °C of this temperature are not important when the uncertainty from other assumptions is considered. Variation of properties under elevated pressure was also not taken into account, with tabulated values at 1 atm even though absolute pressure during the experiment was closer to 2 atm.

The velocity of the coolant was estimated at 1 m/s based on research in the field of coolant heat transfer [52-55]. Similarly, the Reynolds number was estimated at 10,000, due to the assumption of turbulent internal flow. From the estimated velocity and Reynolds number and known properties, the hydraulic diameter of the water jacket was estimated at about 5.6 mm. The Dittus-Boelter equation was used to determine the Nusselt number from these estimates (Equation 7) [56].

$$\mathrm{Nu}_D = 0.023 Re_D^{0.8} Pr^{0.4} \tag{7}$$

The heat transfer coefficient for convection between the coolant and the outer walls of the combustion chamber was determined to be about 5500 W/m^2-K, which is generally high but appears to be within a reasonable range of water jacket heat transfer coefficients [57]. It was assumed that all convective heat transfer associated with this coefficient was the result of 1D conduction through the chamber walls. The solids, as mentioned above, were treated as 1D plane walls, represented in parallel in a thermal resistance network representation. It was assumed that the inner combustion chamber

surface temperature was uniform, even though in real engines, the cylinder head is hotter than the cylinder liner. This assumption would tend to average the surface temperature variation with respect to ECT between the liner and cylinder head surfaces. The thermal resistances and combustion chamber average wall temperature are shown below (Equations 8 & 9).

$$R_{tot} = \frac{1}{hA_{tot}} + \left[\left(\frac{t_{head}}{k_{Al}A_{head}}\right)^{-1} + \left(\frac{t_{liner}}{k_{Fe}A_{liner,avg.}}\right)^{-1}\right]^{-1} \tag{8}$$

$$T_{w,avg.} = T_{coolant} - \frac{\dot{Q}_{radiator}}{4} R_{tot} \tag{9}$$

In the above equations, *R* is thermal resistance [K/W], *h* is heat transfer coefficient [W/m^2-K], *A* is cross-sectional area [m^2], *t* is wall thickness [m], and *k* is thermal conductivity [W/m-K]. The radiator heat transfer rate is divided by four to obtain the per-cylinder average heat transfer rate.

This rough calculation results in a wall temperature change over the range of ECT of 15 °C and 13° C for the LTC and conventional modes, respectively. This change is in line with experimental wall temperature results for an SI engine undergoing a coolant temperature sweep from 90 °C to 120 °C [1]. The agreement with experimental results suggests the simplifications were not egregious, and it is likely that the magnitude of wall temperature increase is in the low tens of degrees Celsius. It is unlikely that this calculation is, for instance, incorrect by an order of magnitude, which means that there actually is substantially less change in wall temperature for this experiment than for Caton's simulation.

4. RESULTS AND DISCUSSION

4.1. Combustion Phasing

Although the test plan initially called for adjustment of combustion phasing (quantified by CA50) by fine-tuning the start of injection, CA50 actually changed little from observation to observation (Figure 4). Combustion phasing shows no clear trend for the LTC cases, with a slight decrease followed by a slight increase over the range of coolant temperatures. In the conventional mode, increasing ECT tends to increase CA50, but over this ECT range of 30 °C, CA50 changed by only about 1.5 °CA.

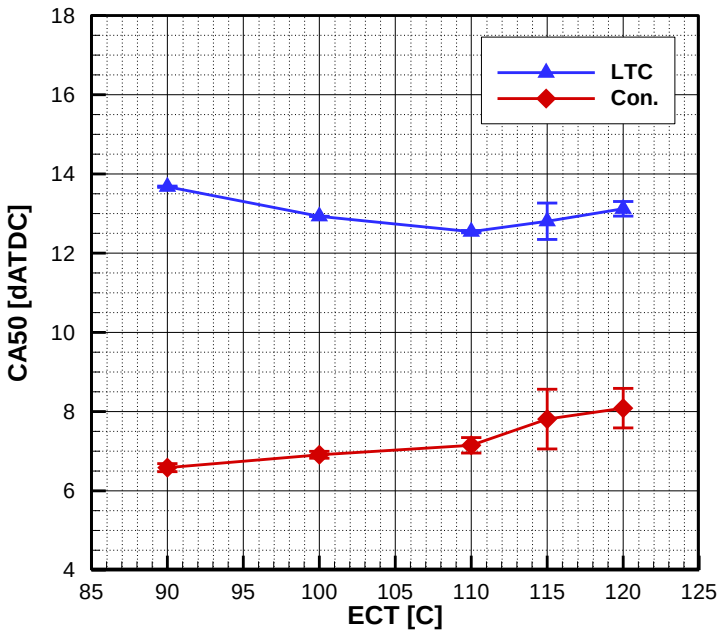

Figure 4: CA50 as a function of ECT.

Out of a combustion durations between about 25 and 30 degrees and over the duration of the expansion stroke, this change in CA50 is a small effect. Furthermore, the sensitivity of CA50 to injection timing would mean that fine-tuning start of injection for more closely matched combustion phasing with the given 0.2 °CA resolution of the shaft encoder would not be particularly useful. Put simply, initial expectations that combustion phasing would substantially change with variation in ECT were unfounded, so combustion phasing effects on efficiency are expected to be small.

4.2. Pressure and Heat Release

Measured in-cylinder pressure provides some useful information on its own, but it is really a stepping stone to the calculated apparent ROHR data, which offers even greater insights into in-cylinder phenomena. The in-cylinder pressure for both modes at the two extremes of the ECT range is plotted in Figure 5. Notable effects of the change in ECT are a decrease in peak pressure for the conventional mode and a decrease in ignition delay for the LTC mode (shown by leftward shift of the LTC pressure trace after TDC).

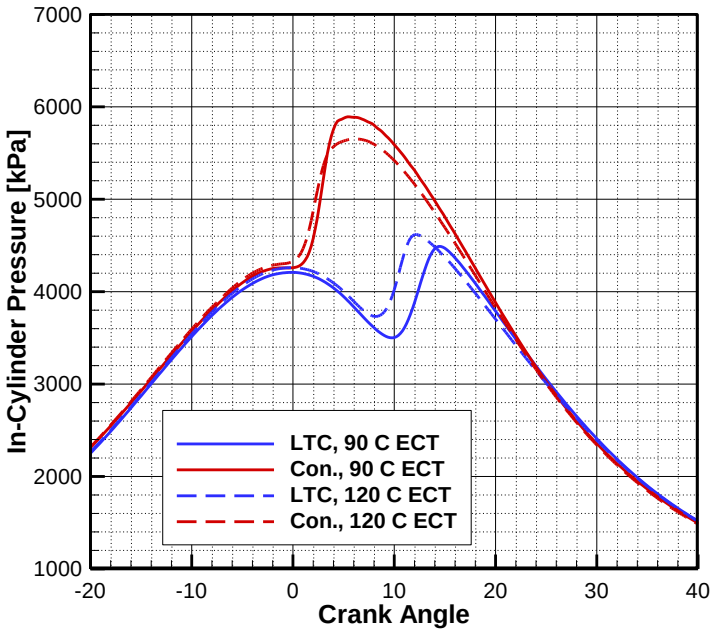

Figure 5: In-cylinder pressure vs. crank angle for both modes at the two ECT extremes.

Using the in-cylinder pressure, known engine kinematics, and estimated wall heat transfer rates as described in ***3.5.2***, the apparent ROHR in Figure 6 was determined. For the conventional mode, increasing ECT from 90 °C to 120 °C causes a small decrease in ignition delay (less than 0.5 °CA), as well as a pronounced decrease in the peak ROHR in the initial premixed spike. The decrease in premixed combustion is only partially offset by an increase in mixing-controlled combustion (NB: the conventional curve for 120 °C ECT is slightly above the curve for 90 °C during the mixing-controlled portion), with the difference explained later by a reduction of conventional combustion efficiency at high ECT (***4.4.1***).

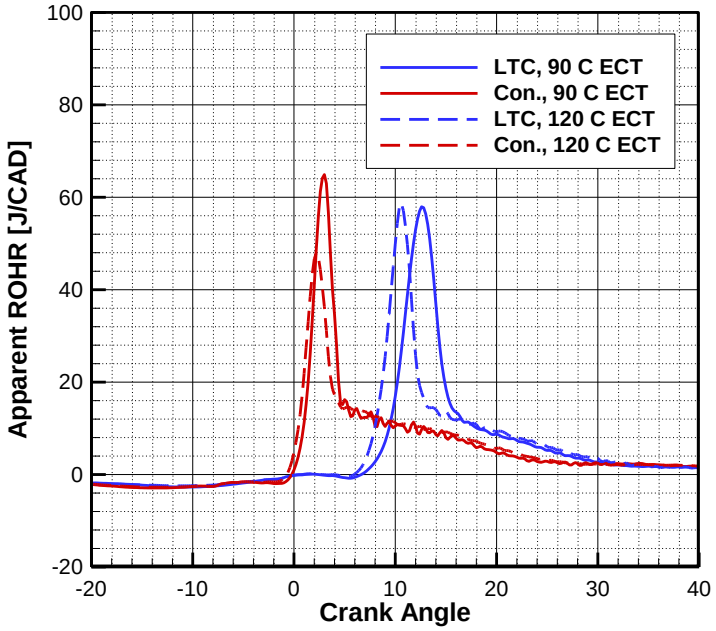

Figure 6: Apparent ROHR vs. crank angle for both modes at the two ECT extremes.

Ignition delay was further shortened for the LTC mode (by about 1 °CA) over the range of ECT. However, the premixed peak is narrower at higher ECT, with greater diffusion burn rate, which explains how CA50 remained nearly constant over the ECT range despite an earlier start of combustion.

For both combustion modes, the changes in ROHR are explained by changes in wall temperatures. Higher wall temperatures translate to higher gas temperatures during injection, which shortens the ignition delay by increasing the propensity for autoignition. This effect is more substantial for the LTC mode because that mode relies heavily on a long ignition delay. Factors which affect ignition delay have more time to affect processes during the longer LTC ignition delay. With the conventional mode ready to

begin combustion near TDC throughout the whole ECT range, the extra impetus to combust given by the increased coolant temperature is not a substantial driver of ignition delay. On the other hand, the LTC mode starts injection near TDC and its ignition delay period encompasses several crank angle degrees of near-constant, minimum volume on either side of TDC. Under those LTC mode circumstances, the change in heat transfer effects on the highly compressed charge is understandably greater as ECT is varied.

4.3. Emissions

An important objective of this study is to quantify changes in emissions from the LTC and conventional modes as LHR operation intensifies. For any comparison of LTC and conventional modes, NO_x and soot should be analyzed to confirm the existence of a nominal LTC condition. For this study, another objective is to seek improvements in CO and THC emissions from the LTC mode relative to the conventional mode through the use of increased ECT.

4.3.1. NO_x and Soot

First and foremost, it was hoped that throughout the test regimen, the primary benefit of LTC combustion could be achieved: substantial reduction in NO_x emissions without a commensurate increase in soot. The defeat of the soot-NO_x tradeoff is the diagnostic hallmark of the low temperature mode. As a first step, NO_x reduction can be quantified by comparison of volume fractions measured by the chemiluminescence analyzer (Figure 7). A substantial reduction in engine-out NO_x concentration was achieved.

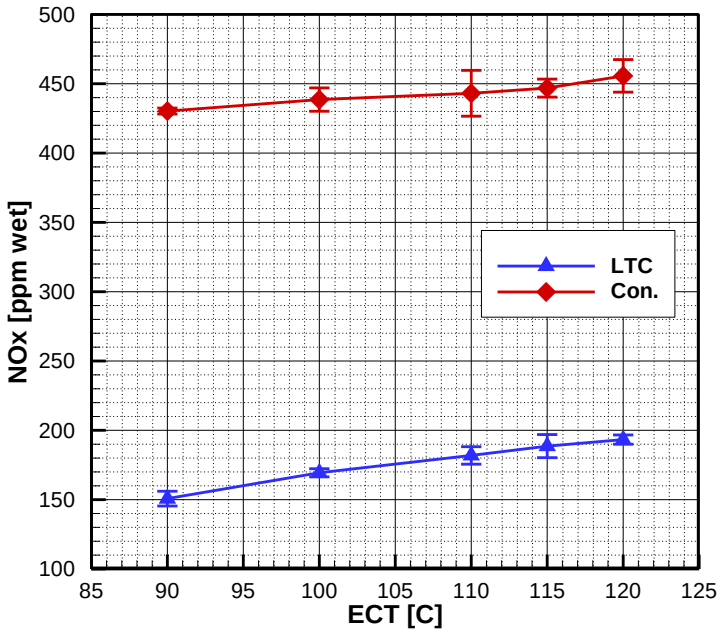

Figure 7: NO_x emissions [ppm] as a function of ECT.

The added EGR and retarded fuel injection substantially reduced the concentration of NO_x in the exhaust for the nominal LTC mode. For both modes, it is also apparent that increasing ECT causes an increase in NO_x. Furthermore, the LTC mode NO_x concentration is marginally more sensitive to increased ECT, while remaining well below conventional concentrations throughout this temperature range.

While exhaust concentration of NO_x has been reduced by the LTC mode, it is also important to consider $BSNO_x$ to verify that the NO_x output per quantity of useful work is likewise controlled under nominally LTC conditions (see ***3.5.1***). $BSNO_x$ is shown in Figure 8, where the LTC mode has indeed caused a drop in specific NO_x by a factor between 3 and 4. This is less of a reduction than what was achieved by Penny,

which is attributable to the reduced EGR fraction during this experiment: EGR is lower (22%) than Penny's target EGR (35%) due to the DAQ and procedural problems mentioned in ***3.4.2.*** However, this is still a useful reduction in NO_x achieved by EGR and retarded injection, and LTC operation can be identified if soot does not significantly increase over the conventional levels.

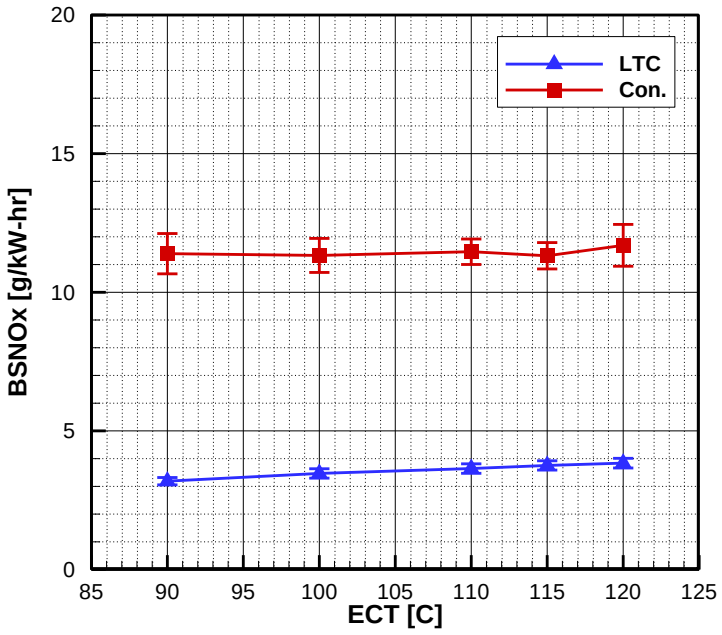

Figure 8: Brake specific NO_x as a function of ECT.

Interestingly, $BSNO_x$ experiences a negligible increase over the range of ECT, in contrast to the volume fraction of NO_x in the exhaust. This implies that brake fuel conversion efficiency increased by the same proportion as NO_x concentration, since the

increase in NO_x concentration must have been canceled out by an increase in useful work during the conversion to $BSNO_x$.

The soot in the exhaust is represented in this study by the FSN, which is plotted in Figure 9. The variance in FSN between the two days was larger than most measurements, suggesting a greater sensitivity of soot formation to ambient conditions and/or less precision with the FSN technique than other emissions measurement methods. A mild LTC mode is confirmed here in light of reduced NO_x, because FSN does not appreciably increase in the switch from conventional to LTC operation. In general, FSN is equal for conventional and LTC modes at each ECT.

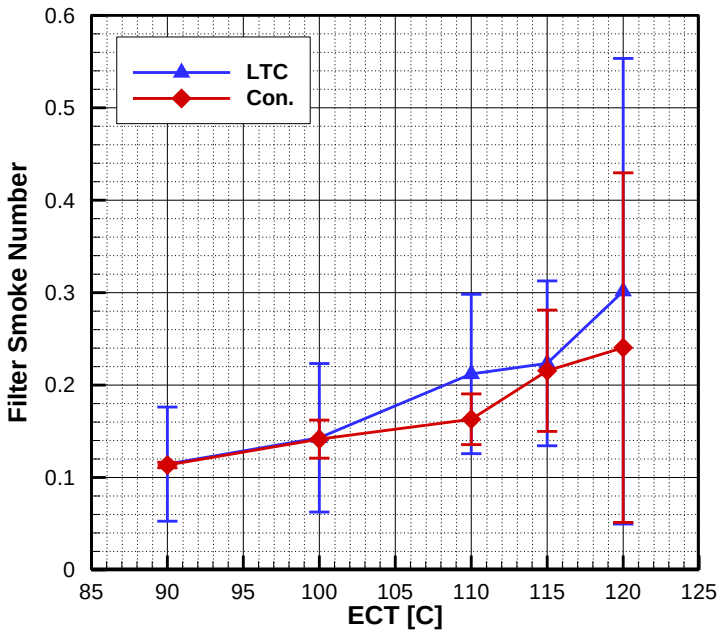

Figure 9: Filter smoke number as a function of ECT.

Additionally, FSN tends to increase with ECT; there are several phenomena that could be involved in this increase. For the LTC mode in particular, increasing wall temperature may contribute to increasing gas temperatures, which can drive net soot formation up from the lower left corner of Figure 1 (***1.2.2***). Since both modes experience similar increases in FSN, however, the stronger phenomenological influence on soot formation could be fuel-air mixing. As the rate of heat release curves showed (Figure 6), ignition delay decreases slightly for the conventional mode and more so for the LTC mode. This in turn changes the proportions of premixed and diffusion combustion, with shorter ignition delay tending to cause more diffusion burn [47]. Diffusion burn contributes to greater soot formation (see ***1.2.2***). From the information provided by traditional experimental techniques, the cause of the increase in Figure 9 cannot be conclusively identified, but optical engine experiments (showing fuel concentration gradients) or validated simulations could shed more light on this.

4.3.2. CO and THC Emissions

Based on the phenomena that cause combustion inefficiency during LTC operation, the LHR strategy was intended to decrease CO and THC emissions for the LTC mode, bringing it more into line with conventional diesel combustion. This objective was realized for CO emissions (Figure 10). Carbon monoxide emissions decrease for each increase in ECT. At the lowest ECT, average LTC CO emissions are almost four times greater than conventional CO emissions. On the other hand, the highest ECT closes that gap by half, to about twice as much CO from the LTC mode than the conventional mode. The reduction in CO for the LTC mode is attributable to

higher wall temperatures, which reduce quenching of the LTC flame near the edges of the combustion chamber [1]. This effect is inconsequential for the conventional mode because its hotter cylinder contents are already at low risk of quenching.

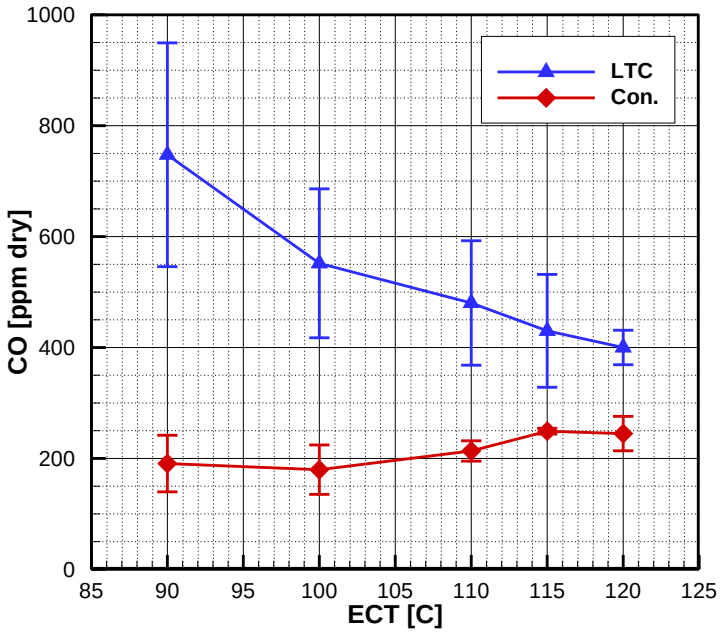

Figure 10: Carbon monoxide concentration as a function of ECT.

For the conventional mode, increasing ECT left CO emissions almost unchanged. The slight increase in conventional mode CO for the highest coolant temperatures is an interesting aberration from expectations. Conventional CO may increase for the highest ECT levels because of a slight reduction in charge density. With the engine components running at higher temperatures, intake mass flow is slightly reduced while fuel injection

remains constant. A slight richening of the (still lean) mixture could cause this slight increase in CO.

The story is more complicated for hydrocarbon emissions (Figure 11). Uncertainty in the LTC mode is high, suggesting that completeness of combustion depended more on day-to-day ambient changes for the LTC mode than for the conventional mode. The LTC mode's greater sensitivity may be related to equilibrium reactions for the hydrocarbons in the presence of different levels of ambient humidity or small changes in equivalence ratio due to changes in daily barometric pressure. Regardless of daily variation, the confidence intervals suggest greater THC from LTC than from conventional operation for the lower ECT levels.

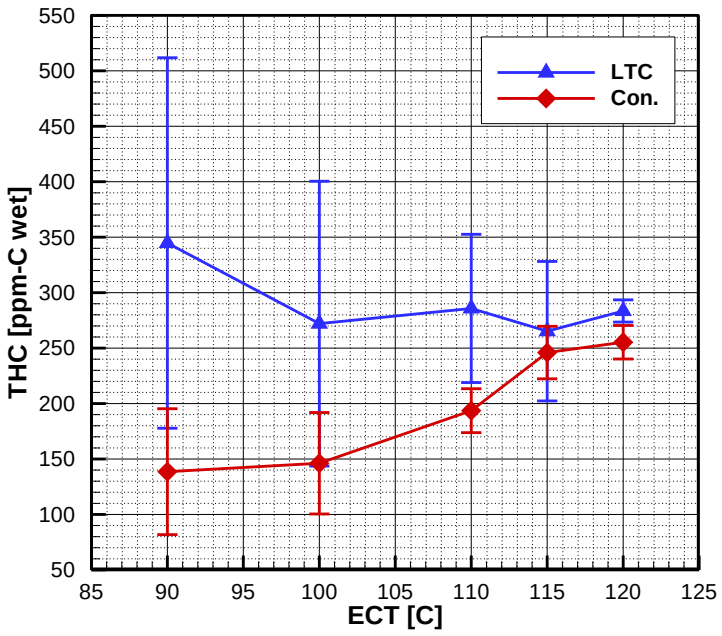

Figure 11: Total hydrocarbon emissions on a per-carbon basis as a function of ECT.

As ECT increases, there is not a significant difference between the two modes' THC concentrations. For the two highest coolant temperatures, LTC THC emissions are not substantially higher than conventional THC emissions. However, this is not entirely satisfying (in terms of reducing the drawbacks of LTC operation) because conventional THC concentration increases by about 50% over the tested range of ECT. The parity between LTC and conventional THC emissions is at least as attributable to increasing conventional concentrations as it is to decreasing LTC concentrations.

The decrease in LTC hydrocarbon emissions is probably explained by the same phenomenon behind LTC CO emissions: quenching around the edges of the combustion chamber decreases when wall temperatures increase [1].

The increase in conventional hydrocarbon emissions may be due to the change in the fractions of premixed and diffusion combustion between the two extremes of ECT, which lead to increased wall wetting for higher coolant temperatures as premixed combustion decreases [58]. On the other hand, one would expect the higher wall temperatures to reduce quenching (as noted in the LTC cases) and to increase other hydrocarbon oxidation mechanisms after combustion, which would tend to maintain or decrease THC emissions from the conventional mode as ECT increases [58-60]. Alternatively or in a contributing role, the higher coolant temperatures could lead to an environment where lubricating oil vaporization impacts measured hydrocarbons [58, 60].

4.4. Efficiencies

This study is also intended to search for improvements in LTC efficiency attributable to LHR operation. Combustion efficiency, brake thermal efficiency, brake

fuel conversion efficiency, net indicated thermal efficiency, and mechanical efficiency provide different information about LHR effects on cycle performance for the two modes.

4.4.1. Combustion Efficiency

Combustion efficiency has already been mentioned in the preceding discussion of ROHR as well as CO and THC emissions. Because diesel combustion is traditionally very nearly complete, in contrast to SI engines, the fairly small reduction in combustion efficiency associated with the LTC mode can have an important negative effect on fuel conversion efficiency.

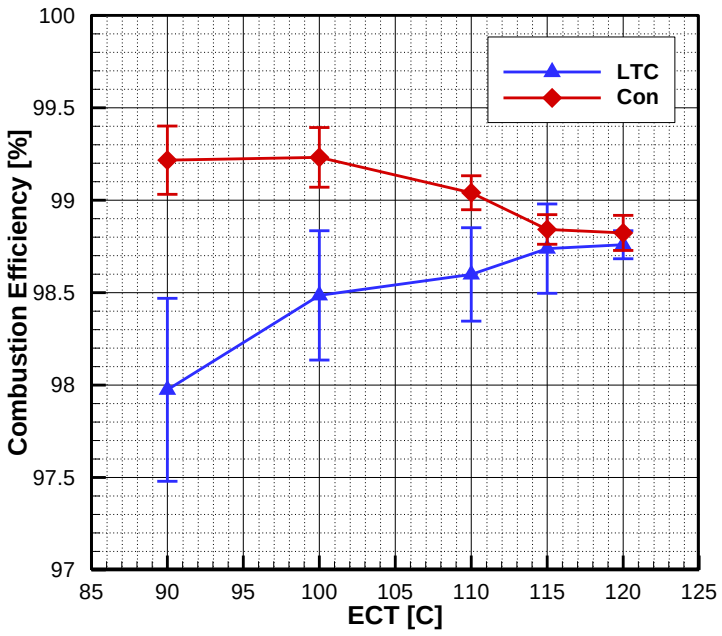

Figure 12: Combustion efficiency as a function of ECT.

As expected, for normal coolant temperatures, LTC combustion efficiency is worse than conventional combustion efficiency. However, as ECT is increased, the LTC mode improves and the conventional mode worsens. Ultimately, for the two highest ECT levels, combustion efficiency is indistinguishable between the two modes. The changes in both modes are explained by the phenomena behind their CO and THC emissions (***4.3.2***). From the lowest to the highest ECT, the LTC mode is improved by about the same amount that the conventional mode is degraded.

Similar to the effect observed in the THC concentrations, it is desirable that the LTC mode sees improvements with the LHR technique, but it is undesirable that parity between the modes is only achieved by degradation of the conventional mode's combustion efficiency. The combustion efficiency drawback of the LTC mode has been reduced, but not eliminated by this LHR technique.

4.4.2. Net Indicated Thermal Efficiency

The net indicated thermal efficiency is the ratio of the boundary work transferred to the piston throughout the entire cycle to the heat released by combustion. This represents the thermal efficiency of the cycle without accounting for frictional losses and including the pumping work transfer during the open portion of the cycle [1]. Net indicated thermal efficiency is shown in Figure 13.

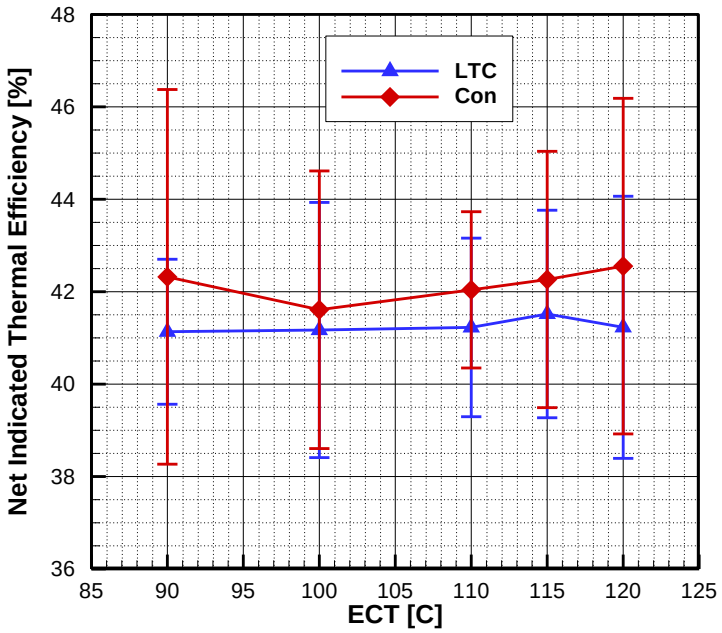

Figure 13: Net indicated thermal efficiency as a function of ECT.

Because of the uncertainty introduced by instrument imprecision and day-to-day ambient effects, the net indicated thermal efficiency cannot be said to be significantly different for the two modes. Based on insights into LTC from the literature review, it is likely that the conventional mode is indeed more efficient by this metric, but this data alone cannot confirm that. This data does suggest that changes in net indicated thermal efficiency with respect to ECT are unimportant in this range; both modes have uncertainties at each ECT level far larger than the observed changes between the ECT levels.

Net indicated thermal efficiency would show evidence of the gas specific heat hypothesis for LTC-LHR efficiency as proposed by Caton [10]. The hypothesis that the

LTC mode's higher ratio of specific heats allows greater conversion of thermal energy to work is not confirmed by this data, but it is not disproved either. Compared to Caton's study with a simulated wall temperature change of a few hundred degrees Celsius, this experiment likely increased wall temperature by about 15 °C (***3.5.4***). Over this relatively small increase in LHR behavior, the positive effect of LTC specific heat ratio on thermal efficiency is simply too small to observe. Furthermore, a more aggressive LTC mode with higher EGR fraction may be needed to capitalize further on the specific heat advantage of lower gas temperatures.

4.4.3. Mechanical Efficiency

The mechanical efficiency is the ratio of the brake work recorded at the dynamometer to the gross indicated work (done by the cylinder contents on the piston during the closed portion of the cycle) [1]. Mechanical efficiency reveals the losses in useful work due to friction in the engine, as well as the pumping work during the open portion of the cycle. In this engine test cell, many accessories are driven electrically, rather than belted to the crankshaft (with the notable exception of the high-pressure fuel pump). Therefore, mechanical efficiency shown here is higher than it would be for a similar engine with a greater number of mechanically driven pumps and fans.

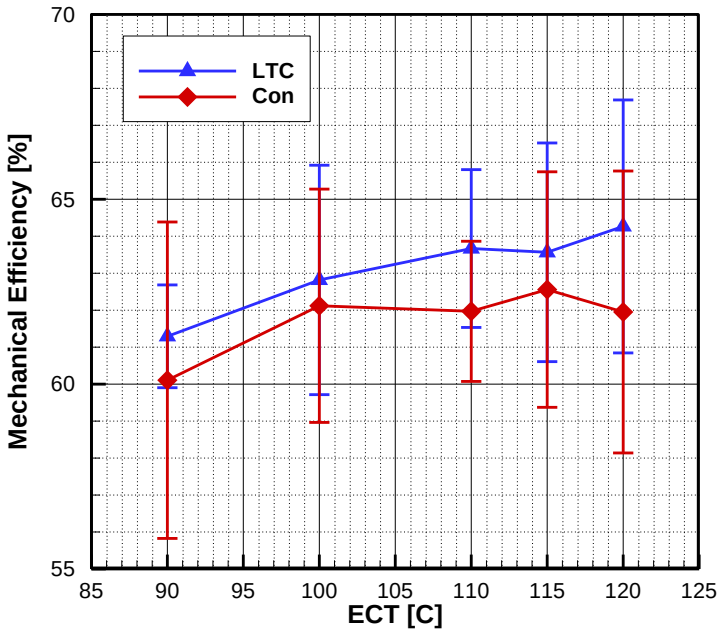

Figure 14: Mechanical efficiency as a function of ECT.

As with net indicated thermal efficiency, the mechanical efficiencies of the two modes are indistinguishable in light of uncertainty. There may be an improvement in mechanical efficiency between 90 °C and 120 °C coolant temperatures, but it is not self-evident, given the overlaps in the error bars. The apparent variation in mechanical efficiency is largely conveyed by variation in pumping work, normalized as PMEP (Figure 15).

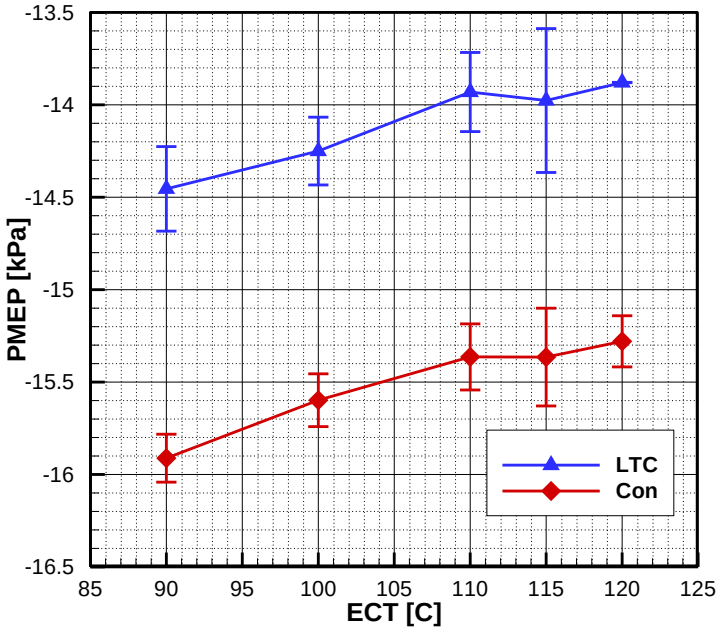

Figure 15: PMEP as a function of ECT.

PMEP becomes more negative as more work is consumed by the control volume to pump gases during the open portion of the cycle. With that understanding, Figure 15 shows an improvement in PMEP as ECT increases for both modes, which mirrors the suspected improvement in mechanical efficiency.

PMEP is better in the LTC mode than the conventional mode because of the flow of EGR. Opening the EGR valve uses the exhaust pressure to displace some intake air (that would otherwise consume pumping work) with exhaust gases.

4.4.4. Brake Thermal Efficiency

Brake thermal efficiency is the ratio of the brake useful shaft work to the heat released by combustion. Brake thermal efficiency reveals, after frictional and pumping

losses, how much of the energy released during combustion was converted to useful work. In Figure 16, the data reveals statistically indistinguishable brake thermal efficiency between the two modes throughout the range of ECT.

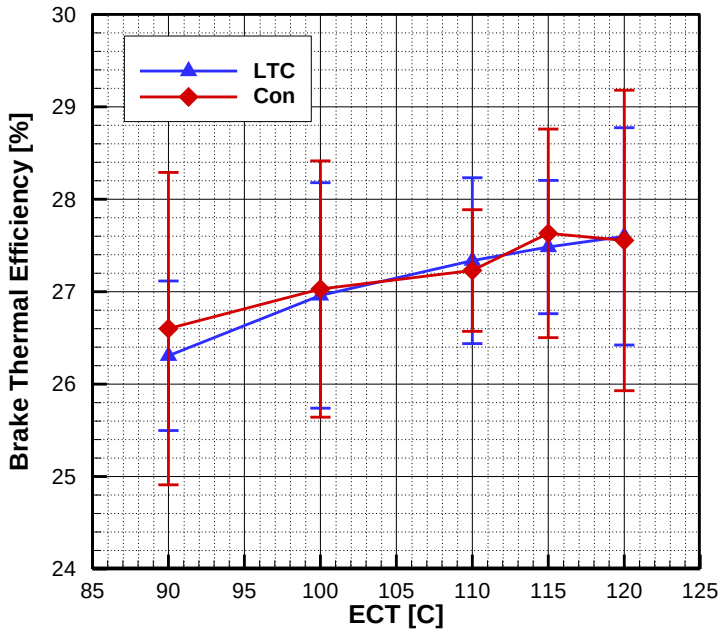

Figure 16: Brake thermal efficiency as a function of ECT.

Brake thermal efficiency is observed to increase as ECT increases, but not by a large amount relative to the uncertainty from point to point. Since indicated thermal efficiency appears rather flat and mechanical efficiency likely shows an improvement due to reduced pumping work, the improvement in brake thermal efficiency can be linked most strongly to the improvement in pumping work.

4.4.5. Brake Fuel Conversion Efficiency

Brake fuel conversion efficiency, the ratio of brake useful power to the rate of

chemical energy delivered to the engine, provides the broadest overall look at engine efficiency. Brake fuel conversion efficiency differs from brake thermal efficiency because of combustion efficiency. Thermal efficiency compares work to the thermal energy released by combustion, whereas fuel conversion efficiency compares work to the chemical energy supplied to the engine. The brake fuel conversion efficiency increases slightly over the range of ECT, although meaningful differences at and between each level are obscured by propagated uncertainty (Figure 17).

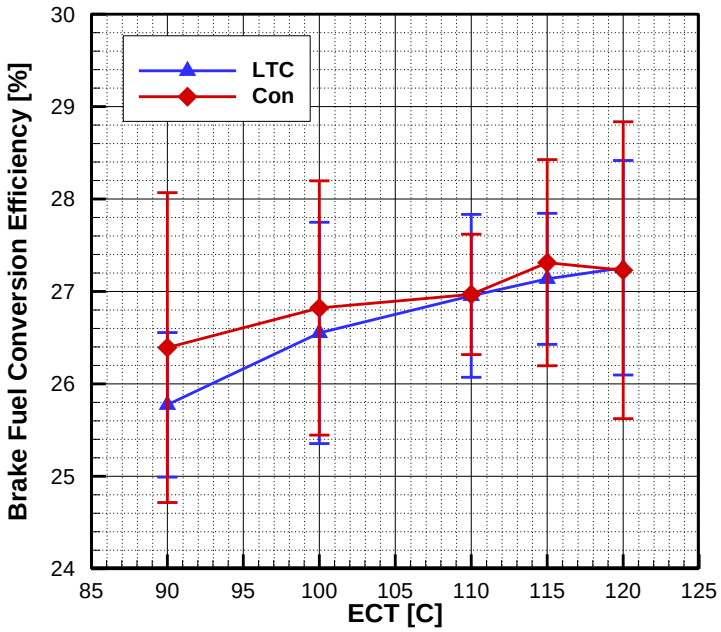

Figure 17: Brake fuel conversion efficiency as a function of ECT.

Because brake fuel conversion efficiency is the product of combustion efficiency and brake thermal efficiency, the combination of those analyses explains its behavior.

The same apparent increase (taking uncertainty into account) of brake thermal efficiency for both modes is visible here, with reduced pumping work playing a role as ECT increases. In light of the uncertainty associated with brake fuel conversion efficiency, the possible reduction in a gap between LTC and conventional brake fuel conversion efficiencies as ECT increases can be attributed to the confirmed behavior seen in their combustion efficiencies (Figure 12).

4.5. Exhaust Temperature and Flow Rate

Apart from work and heat transfer, energy flows out of the test cell through the enthalpy of the flowing exhaust gases. Specific enthalpy is a function of temperature, and the exhaust compositions (dominated by CO_2, H_2O, O_2, and N_2) and temperatures of both modes' exhausts are similar enough that the modes' specific heats are approximately equal (with the caveat that some exhaust species such as CO and THC emissions can have an outsized effect on exhaust enthalpy, although these are present in small concentrations). Figure 18 shows the absolute temperature of the exhaust streams, which is proportional to their specific enthalpies.

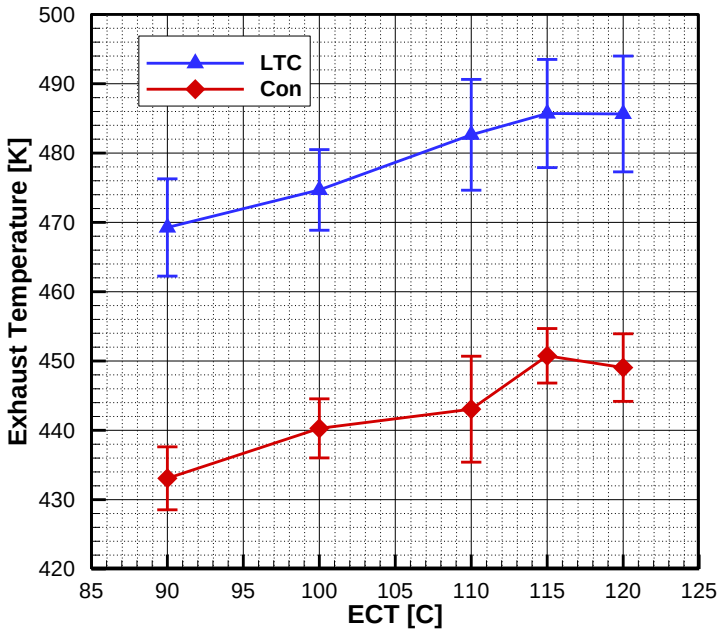

Figure 18: Exhaust manifold temperature as a function of ECT.

The difference in exhaust specific enthalpy between the two modes is at first counterintuitive, considering the rough equivalence in their efficiencies. One might expect the LTC mode's higher exhaust temperature to hint at a lower thermal efficiency, but this difference is actually explained by the use of EGR. For the LTC mode, the EGR which enters during the intake stroke has substantially more thermal energy than pure intake air. Compared to the conventional mode, the LTC mode traps more thermal energy in the cylinder when the intake valves close.

Consider two identical, adiabatic piston-cylinder arrangements containing inert gases. If the initial temperature at the start of compression was the only difference between these two systems, then that temperature difference would remain, unchanged,

at the end of expansion. This is essentially what happens with the inert EGR in the LTC mode, except for some heat losses associated with the hot EGR during the cycle. Despite heat transfer, some additional thermal energy from the EGR remains in the cylinder contents when the exhaust valves open.

Figure 19 provides the exhaust mass flow rates. The relative energy in the exhaust of the two modes is approximated by the product of exhaust temperature and mass flow rate.

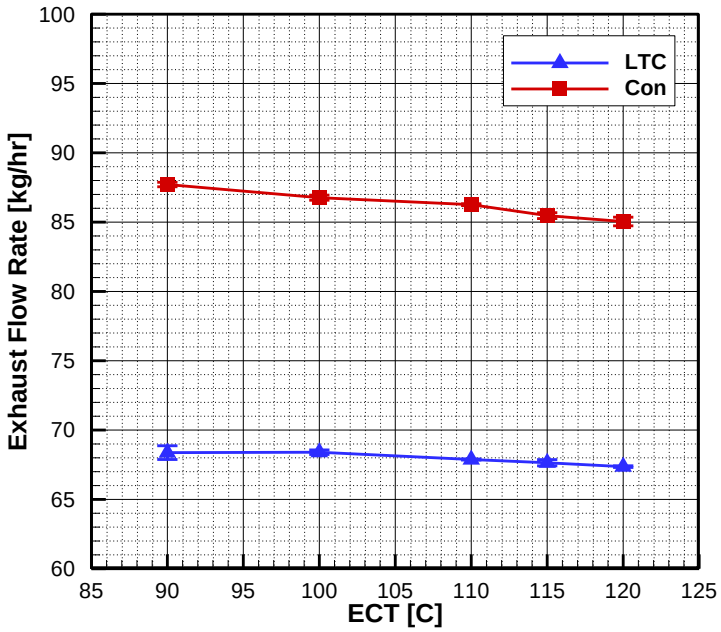

Figure 19: Exhaust flow rate as a function of ECT.

The LTC mode has about 10% higher exhaust temperatures than the conventional mode across the range of ECTs, but it has about 20% lower exhaust flow rates.

Therefore, energy leaving the engine through the exhaust is lower for the LTC mode in this study.

5. SUMMARY AND CONCLUSIONS

This study sought to validate proposed improvements to LTC operation by the integration of an LHR technique. Major drawbacks of the LTC mode under normal conditions include degraded combustion efficiency (which leads to increased CO and THC emissions) and, in many cases, reduced thermal efficiency. The LHR strategy used elevated engine coolant temperatures to reduce the temperature gradient between the cylinder contents and the combustion chamber surfaces.

A mild LTC mode was achieved which defeated the soot-NO_x tradeoff through the use of EGR and retarded fuel injection. Compared to the conventional combustion mode at any given coolant temperature, the mild LTC mode yielded the desired outcomes of reduced NO_x emissions (roughly 70% reduction) without increased soot emissions. This LTC mode also suffered the expected drawback of reduced combustion efficiency. However, the LHR technique improved the combustion efficiency of the LTC mode, reducing its CO and HC emissions by 46% and 18%, respectively.

Conclusions about other efficiency metrics are less clear due to the small difference between experimental averages and the relatively high uncertainty compared to those differences. Neither net indicated nor brake thermal efficiency was substantially lower for the mild LTC mode. No substantial change was observed for either mode's net indicated thermal efficiency as ECT increased. The brake thermal efficiency increased with ECT for both modes, which was attributable to reductions in pumping work as ECT increased.

Because the LTC treatment was so mild in this study, future work should include more aggressive application of EGR, at or above 35%. While this study demonstrated that the soot-NO_x tradeoff can be defeated during LHR operation and that the LHR technique can improve LTC combustion efficiency, it did not verify that LHR can help LTC overcome reductions in thermal efficiency. Two factors are likely contributing to this inconclusive behavior. First, a more aggressive LTC mode would have a higher ratio of specific heats in the cylinder, which would increase the maximum possible thermal efficiency of the cycle compared to this study's mild LTC mode. Second, the LHR technique only increased coolant temperature by a maximum of 30 °C. A different technique involving ceramic coatings or inserts in the combustion chamber could have more dramatic LHR effects which might better realize the hypothesized gains in LTC thermal efficiency.

REFERENCES

[1] Heywood, J. B., 1988, Internal Combustion Engine Fundamentals, McGraw-Hill, Inc., New York, NY.

[2] Jacobs, T. J., and Assanis, D. N., 2007, "The Attainment of Premixed Compression Ignition Low-Temperature Combustion in a Compression Ignition Direct Injection Engine," Proc. The Combustion Institute, Elsevier, pp. 2913-2920.

[3] Lechner, G. A., Jacobs, T. J., Chryssakis, C. A., Assanis, D. N., and Siewert, R. M., 2005, "Evaluation of a Narrow Spray Cone Angle, Advanced Injection Timing Strategy to Achieve Partially Premixed Compression Ignition Combustion in a Diesel Engine," SAE Technical Paper No. 2005-01-0167, SAE International, Warrendale, PA.

[4] Jacobs, T. J., Bohac, S. V., Assanis, D. N., and Szymkowicz, P. G., 2005, "Lean and Rich Premixed Compression Ignition Combustion in a Light-Duty Diesel Engine," SAE Technical Paper No. 2005-01-0166, SAE International, Warrendale, PA.

[5] Bittle, J. A., Knight, B. M., and Jacobs, T. J., 2010, "Investigation Into the Use of Ignition Delay as an Indicator of Low-Temperature Diesel Combustion Attainment," Combustion Science and Technology, 183(2), pp. 138-153.

[6] Turns, S. R., 2012, An Introduction to Combustion: Concepts and Applications, McGraw-Hill, New York, NY.

[7] Ban-Weiss, G. A., Chen, J. Y., Buchholz, B. A., and Dibble, R. W., 2007, "A Numerical Investigation into the Anomalous Slight NO_x Increase When Burning Biodiesel: A New (Old) Theory," Fuel Processing Technology, 88(7), pp. 659-667.

[8] Penny, M. A., 2014, "Efficiency Improvements with Low Heat Rejection Concepts Applied to Low Temperature Combustion," M.S. thesis, Texas A&M University, College Station, TX.

[9] Jacobs, T. J., 2005, "Simultaneous Reduction of Nitric Oxide and Particulate Matter Emissions from a Light-Duty Diesel Engine using Combustion Development and Diesel Oxidation Catalyst," PhD, University of Michigan, Ann Arbor.

[10] Caton, J. A., 2011, "Thermodynamic Advantages of Low Temperature Combustion (LTC) Engines Using Low Heat Rejection (LHR) Concepts," SAE Technical Paper No. 2011-01-0312, SAE International, Warrendale, PA.

[11] Alriksson, M., and Denbratt, I., 2006, "Low Temperature Combustion in a Heavy Duty Diesel Engine Using High Levels of EGR," SAE Technical Paper No. 2006-01-0075, SAE International, Warrendale, PA.

[12] Kokjohn, S. L., Hanson, R. M., Splitter, D. A., and Reitz, R. D., 2009, "Experiments and Modeling of Dual-Fuel HCCI and PCCI Combustion Using In-Cylinder Fuel Blending," SAE Technical Paper No. 2009-01-2647, SAE International, Warrendale, PA.

[13] Epping, K., Aceves, S., Bechtold, R., and Dec, J. E., 2002, "The Potential of HCCI Combustion for High Efficiency and Low Emissions," SAE Technical Paper No. 2002-01-1923, SAE International, Warrendale, PA.

[14] Stanglmaier, R., and Roberts, C., 1999, "Homogeneous Charge Compression Ignition (HCCI): Benefits, Compromises, and Future Engine Applications," SAE Technical Paper No. 1999-01-3682, SAE International, Warrendale, PA.

[15] Stanglmaier, R., Li, J., and Matthews, R. D., 1999, "The Effect of In-Cylinder Wall Wetting Location on the HC Emissions from SI Engines," SAE Technical Paper No. 1999-01-0502, SAE International, Warrendale, PA.

[16] Roberts, C., and Matthews, R. D., 1996, "Development and Application of an Improved Ring Pack Model for Hydrocarbon Emissions Studies," SAE Technical Paper No. 961966, SAE International, Warrendale, PA.

[17] Gray, A. W., and Ryan, T. W., 1997, "Homogeneous Charge Compression Ignition (HCCI) of Diesel Fuel," SAE Technical Paper No. 971676, SAE International, Warrendale, PA.

[18] Iwabuchi, Y., Kawai, K., Shoji, T., and Takeda, Y., 1999, "Trial of New Concept Diesel Combustion System - Premixed Compression-Ignited Combustion," No. 1999-01-0185, Warrendale, PA.

[19] Curran, S., Prikhodko, V., Cho, K., Sluder, C. S., Parks, J., Wagner, R., Kokjohn, S. L., and Reitz, R. D., 2010, "In-Cylinder Fuel Blending of Gasoline/Diesel for Improved Efficiency and Lowest Possible Emissions on a Multi-Cylinder Light-Duty Diesel Engine," No. 2010-01-2206, Warrendale, PA.

[20] Ashley, S., 2010, "Dual-Fuel lab engines achieve high efficiencies, low emissions," Truck & Off-Highway Engineering, SAE International.

[21] Wang, H., DelVescovo, D., Yao, M., and Reitz, R. D., 2015, "Numerical Study of RCCI and HCCI Combustion Processes Using Gasoline, Diesel, iso-Butanol and DTBP Cetane Improver," SAE International Journal of Engines, 8(2), pp. 831-845.

[22] Reddy, C. S., Domingo, N., and Graves, R. L., 1990, "Low Heat Rejection Engine Research Status: Where Do We Go from Here?," SAE Technical Paper No. 900620, SAE International, Warrendale, PA.

[23] Jaichandar, S., and Tamilporai, P., 2003, "Low Heat Rejection Engines - An Overview," SAE Technical Paper No. 2003-01-0405, SAE International, Warrendale, PA.

[24] Jaichandar, S., and Tamilporai, P., 2004, "The Status of Experimental Investigations on Low Heat Rejection Engines," SAE Technical Paper No. 2004-01-1453, SAE International, Warrendale, PA.

[25] Cheng, W. K., Wong, V. W., and Gao, F., 1989, "Heat Transfer Measurement Comparisons in Insulated and Non-Insulated Diesel Engines," SAE Technical Paper No. 890570, SAE International, Warrendale, PA.

[26] Woschni, G., Spindler, W., and Kolesa, K., 1987, "Heat Insulation of Combustion Chamber Walls - A Measure to Decrease the Fuel Consumption of I.C. Engines?," SAE Technical Paper No. 870339, SAE International, Warrendale, PA.

[27] Woschni, G., and Spindler, W., 1988, "Heat Transfer With Insulated Combustion Chamber Walls and Its Influence on the Performance of Diesel Engines," Journal of Engineering for Gas Turbines and Power, 110(3), pp. 482-488.

[28] Nguyen, N. N., 1984, "Über den Einfluss der Wandtemperatur auf die Reaktionsbedingungen in der Grenzschicht und insbesondere auf den konvektiven Wärmeübergang einer Propan-Luft-Flamme," VDI-Fortschrittsberichte, 3(89).

[29] Cheng, W. K., and Wong, V. W., "Does Heat Transfer Increase in Low Heat Rejection Engines? - A Discussion on the Recent Results from Woschni et al.," Proc. 25th Automotive Technology Development Contractors' Coordination Meeting, SAE International, pp. 57-60.

[30] Wade, W. R., Havstad, P. H., Ounsted, E. J., Trinker, F. H., and Garwin, I. J., 1984, "Fuel Economy Opportunities with an Uncooled DI Diesel Engine," Proc. International Conference on Fuel Efficient Power Trains and Vehicles, Mechanical Engineering Publ. Ltd., London, pp. 59-72.

[31] Havstad, P. H., Garwin, I. J., and Wade, W. R., 1986, "A Ceramic Insert Uncooled Diesel Engine," SAE Technical Paper No. 860447, SAE International, Warrendale, PA.

[32] Morel, T., Wahiduzzaman, S., and Fort, E. F., 1988, "LHR Engine Design Analysis Methodology - Heat Transfer Measurements in an Insulated Diesel," SAE Technical Paper No. 880186, SAE International, Warrendale, PA.

[33] Bryzik, W., Schwarz, E. E., Kamo, R., and Woods, M., 1993, "Low Heat Rejection From High Output Ceramic Coated Diesel Engine and Its Impact on Future Design," SAE Technical Paper No. 931021, SAE International, Warrendale, PA.

[34] Annamalai, K., and Puri, I. K., 2007, Combustion Science and Engineering, Taylor & Francis, Boca Raton, FL.

[35] Sigsby, J. E., Black, F. M., Bellar, T. A., and Klosterman, D. L., 1973, "Chemiluminescent Method for Analysis of Nitrogen Compounds in Mobile Source Emissions (NO, NO2, and NH3)," Environ. Sci. Technol., 7(1), pp. 51-54.

[36] Takeda, K., and Koike, H., 1995, "Motor Exhaust Gas Analyzer MEXA-7000 Series: 2. Downsizing and Modular Configuration of Analyzers," Readout, Horiba, pp. 7-13.

[37] Seitz, J., and Tong, C., 2013, "LMP91051 NDIR CO2 Gas Detection System," Application Report No. SNAA207, Texas Instruments.

[38] Silver, J. A., and Chen, S.-J., 2006, "Carbon Monoxide Sensor for Combustion Feedback Control," 44th AIAA Aerospace Sciences Meeting and Exhibit, AIAA, Inc., Reno, NV.

[39] McWilliam, I. G., and Dewar, R. A., 1958, "Flame Ionization Detector for Gas Chromatography," Nature, 181, p. 760.

[40] Halasz, I., and Schreyer, G., 1960, "Erfahrungen mit Kapillarkolonnen-Flammenionisationsdetektor-Systemen bei der Gas-Chromatographie," Chemie Ingenieur Technik, 32(10), pp. 675-685.

[41] Hughes, D. E. P., 1965, "Flame-Ionization Detector for Gas Chromatography," J. Chem. Educ., 42(8), p. 450.

[42] Chasteen, T. G., 2009, "The Flame Ionization Detector," Sam Houston State University, http://www.shsu.edu/~chm_tgc/primers/FID.html.

[43] Halasz, I., and Schneider, W., 1961, "Quantitative Gas Chromatographic Analysis of Hydrocarbons with Capillary Column and Flame Ionization Detector," Analytical Chemistry, 33(8), pp. 978-982.

[44] 2017, "AVL Smoke Meter," AVL LIST, GmbH, https://www.avl.com/-/avl-smoke-meter.

[45] ISO, 1998, "Internal Combustion Compression-Ignition Engines -- Measurement Apparatus for Smoke from Engines Operating under Steady-State Conditions -- Filter-

Type Smokemeter," International Organization for Standardization, Geneva, Switzerland.

[46] EPA, 1997, "Procedures for Preparing Emission Factor Documents," Office of Air Quality Planning and Standards, EPA, Research Triangle Park, NC.

[47] Lyn, W. T., 1963, "Study of Burning Rate and Nature of Combustion in Diesel Engines," Proc. Symposium (International) on Combustion, Elsevier, pp. 1069-1082.

[48] Hohenberg, G. F., 1979, "Advanced Approaches for Heat Transfer Calculations," SAE Technical Paper No. 790825, Warrendale, PA.

[49] Kline, S. J., and McClintock, F. A., 1953, "Describing Uncertainty in Single-Sample Experiments," Mechanical Engineering, 75(Jan.), pp. 3-8.

[50] Moffat, R. J., 1988, "Describing the Uncertainties in Experimental Results," Experimental Thermal and Fluid Science, 1988(1), pp. 3-17.

[51] 1997, "Fluid Properties Calculator," Microelectronics Heat Transfer Laboratory, University of Waterloo, http://www.mhtl.uwaterloo.ca/old/onlinetools/airprop/airprop.html.

[52] Hawley, J. G., Robinson, K., and Campbell, N. A. F., 2001, "IC Engine Coolant Side Heat Transfer - An Experimental Investigation," Journal of the Institute of Energy, 74, pp. 113-123.

[53] Wang, Q., 2009, "Numerical Analysis of Cooling Effects of a Cylinder Head Water Jacket," MS, University of Minnesota Duluth, Duluth, MN.

[54] Kim, D., Hwang, J., Han, S., and Bae, C., 2015, "Effects of Cylinder Head Temperature and Coolant Velocity on the Erosion Behavior of Water Jacket in a Diesel Engine," Wear, 342-343, pp. 117-128.

[55] Makkapati, S., Poe, S., Shaikh, Z., Cross, R., and Mikulec, T., 2002, "Coolant Velocity Correlations in an IC Engine Coolant Jacket," SAE Technical Paper No. 2002-01-1203, SAE International, Warrendale, PA.

[56] Bergman, T. L., Lavine, A. S., Incropera, F. P., and Dewitt, D. P., 2011, Fundamentals of Heat and Mass Transfer, John Wiley & Sons, Inc., Hoboken, NJ.

[57] Liu, B. X., Sun, P., Ning, H. Q., Meng, J., and Huang, H., 2015, "Simulation of Heat Transfer by Fluid Structure Interaction of Diesel Engine Block - Coolant Jacket," Journal of Mechanical Engineering Research and Developments, 38(2), pp. 36-42.

[58] Henningsen, S., 1987, "Evaluation of Emissions and Heat-Release Characteristics from a Simulated Low-Heat-Rejection Diesel Engine," SAE Technical Paper No. 871616, SAE, Inc., Warrendale, PA.

[59] Alkidas, A. C., 1988, "On the Performance and Emissions of an Uncooled Heavy-Duty Single-Cylinder Diesel Engine," SAE Technical Paper No. 880013, SAE, Inc., Warrendale, PA.

[60] Alkidas, A. C., 1989, "Performance and Emissions Achievements with an Uncooled Heavy-Duty, Single-Cylinder Diesel Engine," SAE Technical Paper No. 890144, SAE, Inc., Warrendale, PA.